Title

Direct comparison of fatty acid ratios in single cellular lipid droplets as determined by comparative Raman spectroscopy and gas chromatography

Journal

The Analyst, 138(21)

ISSN

0003-2654 1364-5528

Authors

Schie, Iwan W
Nolte, Lena
Pedersen, Theresa L
et al.

Publication Date

2013

DOI

10.1039/c3an00970j

Peer reviewed

Analyst

RSC Publishing

PAPER

Direct comparison of fatty acid ratios in single cellular lipid droplets as determined by comparative Raman spectroscopy and gas chromatography

Cite this: *Analyst*, 2013, **138**, 6662

Iwan W. Schie,[a] Lena Nolte,[b] Theresa L. Pedersen,[c] Zach Smith,[a] Jian Wu,[d] Idir Yahiatène,[ab] John W. Newman[c] and Thomas Huser*[ab]

Cellular lipid droplets are the least studied and least understood cellular organelles in eukaryotic and prokaryotic cells. Despite a significant body of research studying the physiology of lipid droplets it has not yet been possible to fully determine the composition of individual cellular lipid droplets. In this paper we use Raman spectroscopy on single cellular lipid droplets and least-squares fitting of pure fatty acid spectra to determine the composition of individual lipid droplets in cells after treatment with different ratios of oleic and palmitic acid. We validate the results of the Raman spectroscopy-based single lipid droplet analysis with results obtained by gas chromatography analysis of millions of cells, and find that our approach can accurately predict the relative amount of a specific fatty acid in the lipid droplet. Based on these results we show that the fatty acid composition in individual lipid droplets is on average similar to that of all lipid droplets found in the sample. Furthermore, we expand this approach to the investigation of the lipid composition in single cellular peroxisomes. We determine the location of cellular peroxisomes based on two-photon excitation fluorescence (TPEF) imaging of peroxisomes labeled with the green fluorescent protein, and successive Raman spectroscopy of peroxisomes. We find that in some cases peroxisomes can produce a detectable CARS signal, and that the peroxisomal Raman spectra exhibit an oleic acid-like signature.

Received 15th May 2013
Accepted 15th August 2013

DOI: 10.1039/c3an00970j

www.rsc.org/analyst

1 Introduction

Lipid droplets (LD) are ubiquitous cellular organelles present in all eukaryotes and found in a wide range of sizes and in abundance. As a matter of fact, lipid droplets are even present in prokaryotes.[1] Yet, despite their universal occurrence, lipid droplets are the least studied and least appreciated cellular organelles.[2] Previously, it was assumed that LDs are static energy reservoirs not associated with cellular functions except for those related to lipid homeostasis.[2–4] Recent research has, however, revealed a new, dynamic, and vivid face of this amazing organelle. For example, it has been shown that LDs are associated with cell signaling,[5] protein storage, and degradation.[6] Even more surprisingly, LDs can serve as virus hatcheries, as has been shown in the case of the Hepatitis-C virus.[7–9] Cellular lipid droplets are anything but static.[3] Despite their seemingly important functions, however, LDs are often also associated with negative health effects. For instance, an increased number and size of cellular lipid droplets is frequently associated with obesity, alcoholic and non-alcoholic fatty liver disease (NAFLD), and type II diabetes. Research interest in LDs is vast because a better understanding of this organelle will ultimately lead to a better understanding of the cellular and subcellular pathogenesis of associated diseases.

Various aspects of LD genesis and function have been studied, and many of the associated proteins and their roles in LD homeostasis have been identified.[10] A major and seemingly trivial aspect of LDs has, however, long been neglected or remains difficult to assess: the specific fatty acid composition of individual cellular LDs. This is despite recent research indicating that the composition of single LDs might vary and can influence the type of associated proteins.[6]

The primary tools for studying the composition of lipid droplets are chromatographic methods, which require the extraction of LDs and provide information about lipid type or the amount of a specific fatty acid in LDs. This is typically performed using gas chromatography (GC) or thin layer chromatography (TLC) and a variety of detection systems. A particular problem with these methods, however, is that they produce the total lipid profile or fatty acid profile of all droplets in the sample and do not have the sensitivity to analyze individual LDs. Moreover, these procedures are time consuming, and thus costly.

[a]*Center for Biophotonics, Science and Technology (CBST), University of California, Davis, CA 95817, USA. E-mail: thomas.huser@physik.uni-bielefeld.de; Tel: +49 521 106 5451*

[b]*Biomolecular Photonics, University of Bielefeld, 33501 Bielefeld, Germany*

[c]*Obesity and Metabolism Research Unit, USDA, ARS, Western Human Nutrition Research Center, CA 95616, USA*

[d]*Dept. of Internal Medicine, Division of Gastroenterology and Hepatology, Institute for Regenerative Cures, Sacramento, CA 95817, USA*

In vitro formation of cellular lipid droplets is typically induced by the addition of free fatty acids to the cell culture medium. Two dietary fatty acids representative of saturated and unsaturated fatty acids are palmitic acid and oleic acid, respectively. Several recent studies have investigated the influence of these fatty acids on cells. The widely cited study by Listenberger *et al.*[11] showed that incubation with palmitate acid will cause apoptosis due to palmitic induced lipotoxicity. The suggested mechanism leading to apoptosis is the induced stress on the endoplasmic reticulum caused by this saturated fatty acid.[12,13] On the other hand, when cells are incubated with oleic acid, no significant increase in cell death is observed. Most importantly, when cells are incubated with palmitic acid and oleic acid simultaneously, the palmitate-induced apoptotic responses are absent. This surprising effect was attributed to the initiation of cellular lipid droplet formation by oleic acid, which in turn channels palmitic acid into intracellular lipid droplets, preventing it from causing significant ER stress. This hypothesis has, however, not yet been entirely proven, because no method was able to determine the type and composition of fatty acids in single cellular lipid droplets.

Two emerging techniques of particular interest for lipid research are coherent anti-Stokes Raman scattering (CARS) microscopy and Raman micro-spectroscopy. CARS microscopy has been extensively applied to the study and visualization of LDs in cells and in tissue.[14–18] In particular, CARS microscopy enabled for the first time the rapid label-free visualization of cellular and tissue lipid accumulations with chemical specificity and single cell and single lipid droplet sensitivity. In our own work, we have recently shown that we can quantify the effects of lipolysis products from very low density lipoproteins on cells and determine the average degree of unsaturation in individual cellular lipid droplets based on the analysis of single Raman peak ratios.[18] A similar approach using a compound spontaneous Raman scattering and CARS microscope was also demonstrated by Slipchenko *et al.*[19] By using deuterated palmitic acid they were able to determine the amount of exogenous palmitic acid incorporated into cellular lipid droplets based on the peak intensity of the C–D peak indicative of the deuterated isotope. This approach, however, does not analyze the type of fatty acids present in the cellular lipid droplets, except for the amount of the isotope-labeled exogenous palmitic acid that is incorporated. External fatty acids are, on the other hand, typically not incorporated into cells in their original state, but are often converted to other fatty acid types. Moreover, until now, precise reference data on the ability of Raman spectroscopy to perform a compositional analysis of LDs inside cells with established techniques such as gas chromatography were missing. Thus, to date, it is difficult to assign the specific fatty acid content present in these droplets. In another recent Raman study by Rinia *et al.*[20] the authors used broadband CARS to analyze the peak ratios between C=C vibrations and the CH_2 vibration to visualize the different degrees of fatty acid unsaturation in lipid droplets of adipocytes. This approach proved to work well for the visualization of different phases of fatty acids in cellular lipid droplets, however, the specific type of fatty acid was also not determined.

In this contribution we demonstrate that by combining CARS microscopy with Raman micro-spectroscopy, and least squares (LS) fitting of the Raman spectra from individual lipid droplets to Raman spectra of pure fatty acids, it is possible to determine the percentile amount of a fatty acid of interest in single cellular lipid droplets. By comparing our analysis of the lipid composition in single cellular lipid droplets based on Raman spectroscopy data to results of the lipid composition in lipid droplets from millions of cells based on gas chromatography, we find that our Raman-based approach leads to comparable results in lipid content. At the same time, we show that the composition of individual lipid droplets is reflected in the average composition of many droplets, with some minor variation between droplets, reflecting their individuality. Furthermore, we expand this approach to the investigation of the lipid composition of individual peroxisomes. We locate and identify peroxisomes by labeling them with the green fluorescent protein (GFP), and imaging them by two-photon excited fluorescence (TPEF). We show that a weak lipid CARS signal is generated by some peroxisomes. The Raman spectra acquired from single peroxisomes of interest show that they have a different composition than cellular LDs, *i.e.* ~74% oleic acid.

2 Materials and methods

2.1 Cell culture and treatment

HepG2 cells were grown in DMEM (Sigma-Aldrich Co. St. Louis, MO) containing 10% fetal bovine serum (FBS), 10 mM HEPES, 1% non-essential amino acids, 1% penicillin–streptomycin, in an incubator with 5% CO_2 at 37 °C. Cells were then seeded on glass bottom culture dishes (MatTek Corporation, Ashland, MA), precoated with collagen type I from rat tail (Sigma, St. Louis, MO) at a density of 1×10^5 cells per dish.[21] After 24 hours the cell medium was changed and different ratios of oleic acid (Cayman Chemistry, Ann Arbor, MI), and palmitic acid (Cayman Chemistry, Ann Arbor, MI) complexed with fatty acid free bovine serum albumin (BSA)[11] were added for 24 hours. The fatty acid ratio was varied, but the total FA concentration was kept constant at 500 μM. Cells were then washed twice with 0.01 M phosphate buffered saline (PBS) and fixed in 4% paraformaldehyde at room temperature. For the analysis with Raman spectroscopy and CARS microscopy the fixed cells were kept in 1 mL PBS.

2.2 Peroxisomes staining

Peroxisomes were stained using a commercial transfection kit (CellLight, Peroxisome-GFP, BacMam 2.0, Life Technologies, CA, USA). The staining method is based on a modified baculovirus that contains the DNA sequence of GFP, and peroxisome-specific COOH-targeting sequence, called GFP-PTS1.[22] HepG2 cells were incubated for 24 h with the baculovirus, and were ready for imaging afterwards.

2.3 Compound multiphoton-Raman spectroscopy setup

At the heart of our home-built combined CARS-Raman imaging and spectroscopy system is a picosecond pulsed 1064 nm Nd:YVO4 laser (PicoTrain, HighQ Laser, Austria) with an output

power of 10 W, a repetition rate of 76 MHz, and a pulse duration of 7 ps. The laser pumps two Optical Parametric Oscillators (OPO, Levante, APE Berlin, Berlin, Germany) with a tuning range of 770 nm to 960 nm. This system is described in detail in Schie *et al.*[23] However, several modifications on the scanning side and the detection side were made. The beams are scanned by a pair of galvanometer-actuated mirrors (6215H, Cambridge Technology, Lexington, MA) that allow rapid and flexible steering of the excitation beams. After passing the scanning-mirrors the excitation beams are imaged by two large-diameter lenses (infrared-antireflection-coated achromatic doublets, Thorlabs, Newton, NJ; AC508-200-B, and AC508-250-B) onto the back aperture of the objective lens. The multiphoton signal generated in the sample is collected by a 0.612 NA condenser lens (AL4532-A, Thorlabs, Newton, NJ), which is placed closely above the sample plane. The CARS signal is separated from the TPF signal by a 532 nm dichroic mirror (Semrock, Rochester, NY), and detected on a photomultiplier tube (PMT (H9656-20, Hamamatsu, Japan)), with peak detection sensitivity at 630 nm wavelength, which incorporates a high-voltage power supply circuit and a custom-made 20 MHz low noise amplifier. The TPF signal is imaged onto a PMT with a GaAsP/GaAs photocathode (H7421-40, Hamamatsu, Japan), and an integrated thermo-electric cooler for a higher quantum efficiency and better *S*/*N* ratio at a peak wavelength of 580 nm. Data acquisition and the galvo-scanning mirrors are controlled by the Matlab® based program ScanImage[24] developed by the group of Karel Svoboda at HHMI Janelia Farm Research Campus.

Our spontaneous Raman scattering spectroscopy setup is based on a 785 nm cw diode laser system (ChrystaLaser, Reno, NV) with an output power of 100 mW. The beam is expanded by a telescope to a diameter of 6 mm. To remove side-wing contributions from the laser source and to ensure monochromatic illumination, the collimated beam passes a narrow 785 nm bandpass filter (Semrock, Rochester, NY). The beam is then combined with the CARS excitation beams by a 785 nm dichromatic longpass filter (Semrock, Rochester, NY). A flip-mirror is located behind the dichroic mirror to send the epi-collected Raman signal generated in the sample to the spectrometer. To enable confocal detection the signal is focused by a 150 mm focal length lens onto a multimode fiber (Thorlabs, Newton, NJ) with 105 μm core diameter and 1 m length, so that the fiber entrance acts as a pinhole. The multimode fiber is connected to an imaging spectrograph (Acton SpectraPro 2300i, PI Acton, Trenton, NJ) that has a switchable grating turret with three different gratings. Typically, a 300 groove per mm grating is used to disperse the incoming light onto a back-illuminated deep-depletion charge-coupled device camera (PIXIS 100BR, PI Acton, Trenton, NJ).

2.4 Correction of Raman spectra

The acquisition time for the Raman spectra of cellular lipid droplets was 10 s per spectrum. All Raman spectra were equally processed based on an custom-written Matlab®-based algorithm using a modified polynomial fitting procedure as described by Lieber and Mahadevan-Jansen,[25] and automated fitting of known glass background fluorescence spectra based on the Beier and Berger approach.[26] The processed spectra were cropped to remove regions below 500 cm^{-1} and beyond 3200 cm^{-1} and other parts that do not contain information, *i.e.* between 1700 cm^{-1} and 2700 cm^{-1}. It is important to mention that the ester peak located at 1742 cm^{-1} was removed from the analyzed data, because this peak is not present in pure fatty acids, and thus would contribute to an error in the LS analysis. After the spectra were cropped, they were normalized to their total area such that the total area under each spectrum equals one.

2.5 Gas chromatography analysis

Cell pellets washed with PBS were stored at −20 °C for 2 days prior to thaw on wet ice. Thawed samples were doped with an anti-oxidant consisting of 5 μL 0.2 mg per mL BHT–EDTA in 1 : 1 methanol–water (v/v), and deuterated tripalmitoyl-glycerol, and brought to 3 mL with de-ionized water. Deuterated tripalmitoyl-glycerol was introduced into samples as an analytical surrogate to correct for losses of fatty acids during analytical sample preparation. Samples were vortexed for 30 seconds with two 4 mm stainless steel balls to homogenize. Homogenates were transferred to 15 mL polypropylene tubes and subjected to total lipid extraction by 10 : 8 : 11 isopropanol–cyclohexane–0.1 M ammonium acetate (v/v/v) using a slight modification of the Smedes protocol.[27] A 3 mL de-ionized water reagent blank was also prepared according to this protocol. Extracts were dried, solubilized in 400 μL 1 : 1 cyclohexane–isopropanol (v/v), and split in half for GC and Raman analysis. Both aliquots were again evaporated. The aliquot reserved for GC analysis was reconstituted in 1 : 1 methanol–toluene (v/v). Forty microliters of each sample and the blank were doped with C15:1n5 as a derivatization surrogate. An additional derivatization blank was added and doped with deuterium-labeled fatty acids. Samples and blanks were transmethylated at 60 °C with dry methanolic sodium hydroxide, neutralized with potassium carbonate, and extracted with hexane. A 10 μL portion of this extract was diluted with 90 μL of 44 μM of C23:0 methyl ester in hexane prior to GC analysis of methyl-ester derivatives of palmitic and oleic acid. The inclusion of C23:0 methyl ester allows for an accurate calculation of the extraction surrogate recovery and provides a consistent relative retention time lock to enhance confirmation of analytical targets. The isolated fatty acid methyl esters were analyzed by GC/MS on a 6890/5973N equipped with a 30 m × 0.25 mm × 0.25 μm DB-225ms capillary column (Agilent Technologies). Lipids were ionized by electron impact and data was collected in simultaneously selected ion monitoring/full scan mode. Quantification was based on 7-point calibration curves of selected ion monitoring signals from authentic standards.

2.6 Least squares fitting methods

All least squares fitting calculations were performed using the Matlab Statistics Toolbox.

2.6.1 Ordinary least squares (OLS) fitting. Raman spectra are often modeled as a superposition of pure spectra arising

from the individual chemical components of the sample. In other words, a linear model of the form:

$$\mathbf{s} = \mathbf{Pc} + \varepsilon, \quad (1)$$

where **s** is the spectrum of the sample, **P** is a matrix where each row corresponds to a spectrum of a pure component, **c** is a vector of concentrations for each of these components, and ε is the noise contained in the measurement. In the case where all components of the sample are known, the ordinary least squares approach can provide quantitative information about chemical components within samples with a very high degree of accuracy.[28,29] There are, however, many cases for which it is difficult or impossible to construct a truly accurate least squares model, due to significant contributions to the measured spectrum from unknown chemical components which may introduce errors in the fitting process that lead to negative concentration values.

2.6.2 Non-negative least squares (NNLS) fitting. Ordinary least squares does not restrict the concentration values to be positive, which can make it unsuitable for handling real measurements, since negative concentration values are meaningless. Non-negative least squares fitting puts a constraint on the least squares algorithm to only allow positive values for the concentration **c**. NNLS has previously been used to determine concentration values based on Raman spectra,[29,30] giving superior results compared to OLS by preventing over-fitting in the model.

2.6.3 Asymmetric least squares (AsLS) fitting. A traditional least squares model assumes a residual composed of zero-mean Gaussian-distributed noise, and minimizes an unweighted sum-squared error. The AsLS technique,[31] by contrast, minimizes

$$f = \sum_{i=1}^{n} w_i r_i^2, \quad (2)$$

where n is the number of wavenumbers in the spectrum, r_i are the elements of the residual vector $\mathbf{r} = \mathbf{s} - \mathbf{Pc}$, and w_i are the elements of a weight vector **w**. Each element is set to a scalar p ($0 < p < 1$) for positive residuals, and $1 - p$ for negative residuals. In this work we set $p = 0.1$, heavily penalizing negative residuals. In our case, where unmodeled components are present in the residual, the residual is not expected to be zero-mean, but rather positive-definite to within the level of noise. Therefore, using the AsLS approach resulted in more sensible models of the data, with more physical residuals, compared to an ordinary least squares (OLS) modeling approach.

2.6.4 Weighted least squares (WLS) fitting. The OLS model uses the assumption that every measured point contributes equally precise information of a measurement. This, however, does not hold in most cases. Therefore, it is helpful to introduce a weighting-function that gives less precise information a lower value and more precise information a higher value. This can be achieved by weighing each wavelength value with the inverse of its variance.

3 Results and discussion

Before investigating whether LS analysis of cellular lipid droplets can extract information about the relative amount of a particular fatty acid, we wanted to validate this approach on a simple mixture of fatty acids with known fatty acid composition. Therefore, we prepared a mixture of two common unsaturated dietary fatty acids, oleic acid and linoleic acid, and acquired 10 Raman spectra from this fatty acid mixture. Fig. 1a, shows Raman spectra for pure oleic acid, pure linoleic acid, and a 50/50 mixture of the two. The observed spectral differences are correlated to the differences in degree of bond unsaturation of the fatty acids. Oleic acid and linoleic acid each have an aliphatic tail of 18 carbon atoms with one and two unsaturated double bonds, respectively. The assignments of the Raman peaks and their corresponding molecular bond vibrations can be found in ref. 32.

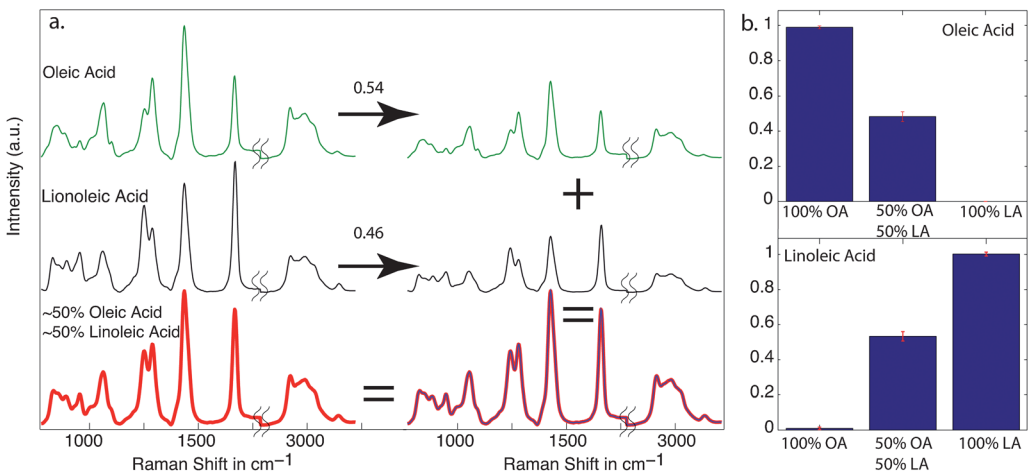

Fig. 1 (a) The left-hand side of the figure shows the Raman spectra of pure oleic acid (OA), linoleic acid (LA), as well as a spectrum of a 50/50 mixture of the two fatty acids. The spectrum of the mixture shows the features of both fatty acids. When applying least squares fitting to the spectra of the mixed fatty acids, the percentile amount of the pure fatty acid contributions to the spectra are retrieved. For the 50/50 mixture this results in a value of 0.54 for OA and 0.46 for LA. By multiplying the original spectra with the determined concentrations and adding them, we obtain the spectrum shown in the lower left-hand corner of the figure. Here, red represents the original and blue represents the calculated spectra of the pure fatty acids. (b) Bar-graphs of the fit results for the spectra of pure oleic acid, linoleic acid, and the 50/50 mixture of the two. The amounts are predicted with high accuracy as seen by the excellent agreement between the values on the *x*- and *y*-axes.

To extract information about the percentile amount of a mixture of oleic and linoleic acid, Raman spectra of the pure fatty acids were acquired. The spectrum of pure oleic acid was later also used to fit the data obtained from single lipid droplet experiments. Since these spectra only contain contributions of the two fatty acids, simple OLS fitting could be applied to their analysis. After OLS fitting the Raman spectra of the mixed sample with the Raman spectra of the two pure fatty acids we determined that the relative amount of oleic acid in the mixture was 0.54 and the relative amount of linoleic acid in the mixture was 0.46. This means that oleic acid contributes with 54% and linoleic acid contributes with 46% to the mixed spectrum. The small deviation from the mixture ratio of 50/50 which we intended to reach is most likely explained by the small volumes used to prepare the mixture (1 μL droplets of the pure fatty acids were used) and the pipetting error related to the small volumes. To show how precisely the algorithm calculated the relative contributions of the pure fatty acids to the mixture we can also multiply the normalized spectra of the pure fatty acids with the calculated concentration values, and then add up the spectra. The resulting spectrum is shown in red in the lower right-hand corner of Fig. 1a. We also measured the Raman spectrum of the mixture and colored it in blue (not shown individually). To compare the calculated and the measured spectra, we plotted their overlay in the spectrum shown in the lower middle of the figure. The purple color of the overlay spectrum shows that the algorithm extracted the relative percentile amount of the fatty acids very accurately and the deviation between the spectra is smaller than the linewidth of the plot. The algorithm was further applied to pure oleic acid and pure linoleic acid, and the predicted values resemble very accurately the known contributions to the mixtures, see Fig. 1b.

Although the combination of oleic acid and linoleic acid represents an interesting model system because both fatty acids are highly abundant in our diet, another fatty acid combination is of particular interest. Two fatty acids very frequently under investigation for their effects on cells are the saturated palmitic acid, C16:0, and the unsaturated oleic acid, C18:1 (ω-9). Both fatty acids are the most common fatty acids found in human diet,[33] and hence, a close examination of their influence on cellular processes is extremely important. Palmitic acid is solid at room temperature, which makes it difficult to create mixtures of palmitic acid and oleic acid, as was done with oleic acid and linoleic acid.

As previously described, oleic acid can rescue cells from palmitate-induced apoptosis by channeling palmitic acid into cellular lipid droplets.[11] However, this mechanism has only been shown by bulk analysis of cellular lipid droplets, due to the detection limitations of gas chromatography. It has, however, never been shown that the proposed mechanism is indeed reflected at the single lipid droplet level. Therefore, to investigate whether the amounts of oleic acid or palmitic acid determined by GC data from bulk samples are also reflected in individual cellular lipid droplets we compared the GC analysis from hundreds of thousand of cellular lipid droplets to the results of Raman spectra of individual cellular lipid droplets.

To determine the types of intracellular fatty acids after incubation with BSA-bound palmitic and oleic acid, 6 dishes, with 2×10^6 cells each, were supplemented with different ratios of the two fatty acids, at 37 °C for 24 h. The total supplemented fatty acid concentration in culture medium was 500 μM. After the incubation time, the cells were washed twice in PBS, and trypsinized to detach them from the glass substrate. The detached cells were then transferred to conventional centrifuge tubes, pelleted, washed twice in PBS, transferred to −80 °C tubes, and frozen until GC analysis. By using gas chromatography more than 11 different types of fatty acids were recovered. However, only three of the recovered fatty acids, palmitic acid, oleic acid and vaccenic acid, were present on average at amounts of >10%. The amounts of palmitic acid and oleic acid were changing according to the treatment, while the amount of vaccenic acid remained fairly constant and independent of the treatment. Table 1 summarizes the percentile amount of the three fatty acids found in the cells for each individual treatment as determined by GC.

Table 1 The amounts of the three fatty acids present at an average ratio >10% within the different treatment protocols using oleic and palmitic acid, as determined by gas chromatography are summarized. All values are given as percentage of the total recovered fatty acid content. The recovered amounts of oleic acid and palmitic acid increase and decrease upon treatment with oleate and palmitate, whereas vaccenic acid remains fairly constant with treatment. In the control sample the amount of oleic acid is similar to vaccenic acid and approximately twice that of palmitic acid

PA in μM	500	400	300	200	100	0	Contr.
OA in μM	0	100	200	300	400	500	Contr.
PA	63.2	53.3	42.2	20.3	5.8	7.4	12.9
OA	9.8	17.9	29.7	51.3	68.6	70.1	27.4
VA	9.4	9.8	12.6	11.7	10.3	8.8	24.4

For the analysis of single cellular lipid droplets with the compound CARS-Raman system, 3 treatments with different ratios of oleic acid and palmitic acid were prepared in the same manner as the cells for the GC analysis. The three treatments were oleic acid only, palmitic acid only, and 250 μM of each fatty acid combined; a control sample of untreated HepG2 cells was prepared as well. After cells were incubated with the fatty acids for 24 h, they were washed in cold PBS twice, and fixed in 4% paraformaldehyde at room temperature. Upon fixation CARS images of the cells were taken and successive Raman spectra of individual cellular lipid droplets observed in the images were recorded. The acquisition time for the Raman spectra was 10 s for each droplet.

The GC analysis of the cellular lipid droplet extracts revealed that palmitic acid, oleic acid and vaccenic acid were present at average concentrations >10%. Vaccenic acid, however, has the same chain length and number of unsaturated bonds as oleic acid, which makes it difficult to distinguish between these two fatty acids based on their Raman spectra. Consequently, the recovered percentile amounts of the two fatty acids were combined and the Raman spectra of both fatty acids were expressed based on the Raman spectrum of pure oleic acid. Therefore, in the data analysis we present the amount of 18:1 fatty acids, comprised of both, oleic acid and vaccenic acid as determined by fitting the data with the spectrum of pure oleic acid. For palmitic acid we took Raman spectra of pure palmitic acid. After establishing the Raman spectra of our compounds of

interest we compared the performance of different least squares fitting methods, *i.e.* ordinary least squares (OLS), non-negative least squares (NNLS), asymmetric least squares (AsLS), and weighted least squares (WLS) fitting to determine the relative contributions of oleic acid and palmitic acid in individual lipid droplets for different treatments. The quality of the prediction of each method was then compared to the corresponding GC values from lipid droplets of 2×10^6 cells, using the root-mean-square error (RMSE); $\mathrm{RMSE} = \sqrt{\frac{\sum_{i=1}^{n} (y_1 - \hat{y}_2)^2}{n}}$.

Fig. 2a and b show the comparison between the different least squares methods and GC analysis for 18:1 fatty acids and palmitic acid, respectively. The LS values are all based on the prediction of the average fatty acid composition of 10 individual lipid droplets, and the GC values are based on the analysis of lipid droplets from 2×10^6 cells. So far it has not been shown whether individual cellular lipid droplets are comprised of different fatty acids, because traditional methods to determine the composition of cellular lipid droplets can only perform the analysis on bulk samples. However, it is safe to assume that even though there will be some variation in the composition between individual cellular lipid droplets, when averaged the composition of individual cellular lipid droplets has to be reflected in the composition of the bulk sample. Therefore, we assessed the quality of least squares fitting methods by comparing the average values of 10 cellular lipid droplets to the GC values from lipid droplets derived from 2×10^6 cells. As a measure of the quality of prediction for each LS method, we calculated the root-mean-squares of error (RMSE) values for the prediction of oleic acid content in each treatment as compared to the values established by GC, and the RMSE values for the prediction of palmitic acid in each treatment as compared to the values established by GC, see Fig. 2c. Each least squares method recovered a value, based on the Raman spectra of individual lipid droplets, that is very close to the value determined by GC analysis from bulk samples, supporting our assumption that the average of several individual lipid droplets should reflect the fatty acid composition of the bulk. Asymmetric least squares (AsLS) fitting performed better in both cases, the prediction of the relative oleic acid content, (RMSE = 0.042), and the prediction of the relative palmitic acid content, (RMSE = 0.036) as shown in Fig. 2c. For the predicted amount of 18:1 fatty acid content and for the predicted amount of palmitic acid, we find that the concentration values deviate only slightly from the values determined by GC analysis. The slight deviations from the GC data, especially when looking at the treatment with mixtures between oleic acid and palmitic acid, can be explained by the presence of other types of unsaturated fatty acids within the lipid droplets, which was also established by GC. Even though the individual amounts of the fatty acids that were not considered in the analysis were small, they can add up when considering all unsaturated fatty acids present, and hence, there will be stronger peaks associated with unsaturated fatty acid bonds. We also applied the one-sample Kolmogorov–Smirnov test, from the Matlab Statistical-Toolbox, with a confidence level of >95% to determine whether our data were normally distributed in each measurement group and each fatty acid type. We found that the concentration of 18:1 fatty acids (oleic acid and vaccenic acid combined) and the concentration of palmitic acid were both normally distributed for the different measurement groups.

In Fig. 3 we show CARS images of HepG2 cells that were exposed to different combinations of oleic acid and palmitic acid, and the fatty acid content determined for individual cellular lipid droplets. Raman spectra were taken from several lipid droplets identified in these images; three lipid droplets are indicated in each image. For each of the indicated lipid droplets

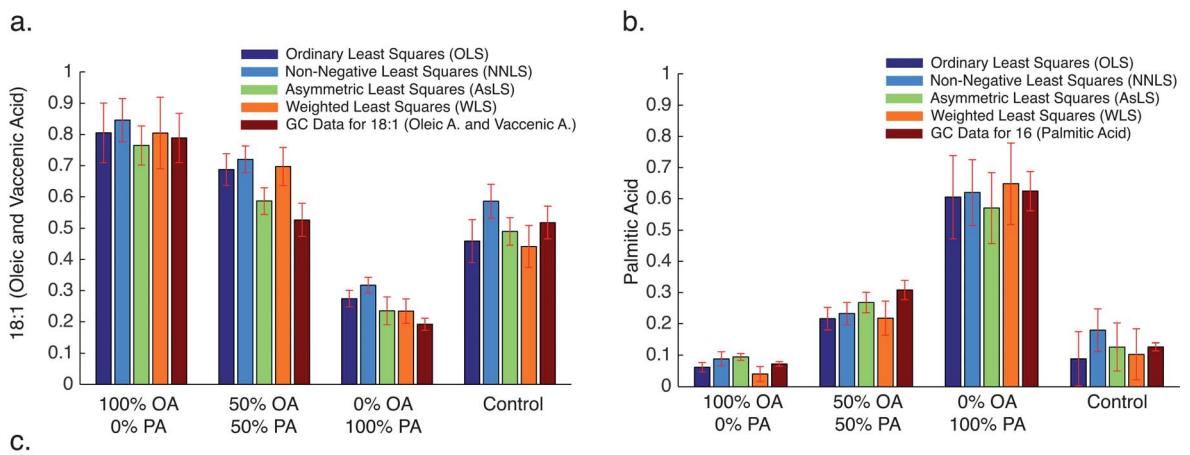

c.

18:1 (OA & VA)	OLS	NNLS	AsLS	WLS	GC
RMSE	0.0954	0.1236	0.0415	0.0961	0

16:0 (PA)	OLS	NNLS	AsLS	WLS	GC
RMSE	0.0515	0.0474	0.0361	0.0514	0

Fig. 2 Comparison between the different least squares fitting methods, *i.e.* ordinary least squares (OLS), non-negative least squares (NNLS), asymmetric least squares (AsLS), and weighted least squares (WLS) fitting to (a) determine the lipid content of 18:1 fatty acids that includes oleic acid 18:1 (ω-9) and vaccenic acid 18:1 (ω-7), in comparison to values obtained by GC, and (b) to determine the lipid content of palmitic acid. (c) Root-mean-squares of error values of the fitting procedures as a measure of performance in comparison to the GC value. AsLS performs better for both fatty acids; GC compared with itself gives a 0 as expected.

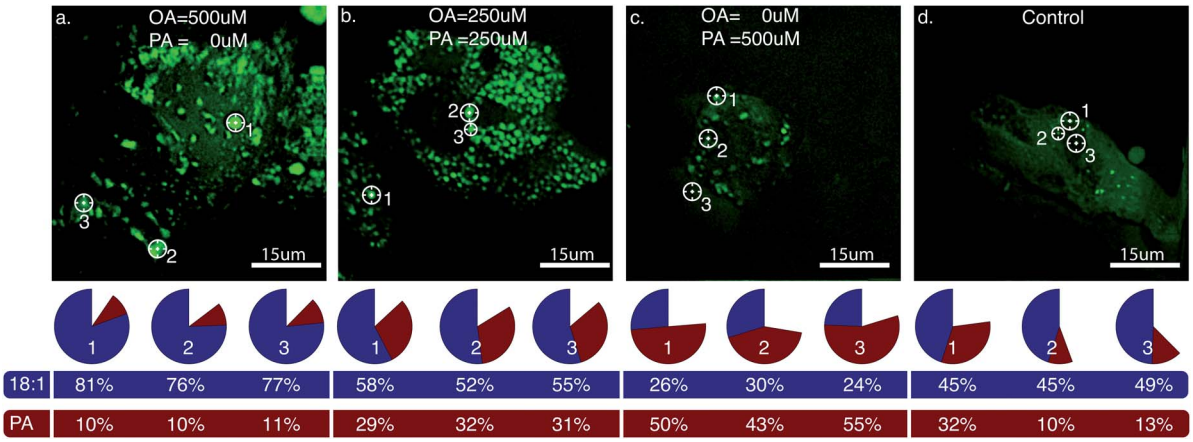

Fig. 3 CARS image of HepG2 cells after a treatment with (a) 500 μM oleic acid; (b) 250 μM oleic acid and 250 μM palmitic acid; (c) 500 μM palmitic acid. (d) Image of control cells. Spontaneous Raman spectra were acquired from the indicated cellular lipid droplets, and the amounts for 18:1 fatty acids and palmitic acid, as calculated by AsLS, were indicated by pie charts, and expressed as numerically below the pie charts.

we show the corresponding composition in terms of 18:1 fatty acids (oleic acid and vaccenic acid combined) and palmitic acid content, as calculated from the Raman spectra using AsLS fitting. The pie chart indicates the relative amount of 18:1 fatty acid and palmitic acid for each indicated lipid droplet; the exact values are written below each pie chart. Fig. 3a shows the CARS image of cells treated with 500 μM oleic acid only. It can be seen that the cells developed significant cellular lipid accumulations, and even very large cellular lipid droplets (>2 μm) could be found. The fatty acid composition values obtained for the three cellular lipid droplets show some minor droplet-to-droplet variation, on the order of 5%, for 18:1 fatty acids, and an almost constant value for palmitic acid. Fig. 3b shows cells treated with a combination of 250 μM oleic acid and 250 μM palmitic acid. Here, the cellular lipid droplets are not as large as the droplets in the case of pure oleic acid. However, one can see that the droplets are more densely packed as compared to the case of pure oleic acid. The values determined for 18:1 fatty acids and palmitic acid content show that even though the cells were supplemented with equal concentrations of both fatty acids, the unsaturated 18:1 fatty acids are present at approx. twice the amount of palmitic acid, indicating substrate preference for 18:1 fatty acids over palmitic acid on the single lipid droplet level. Fig. 3c shows the CARS image of a cell treated with palmitic acid only. It should be mentioned that in contrast to the previous two treatments in this case the majority of cells were not adhering to the glass bottom dish, 24 h after the treatment, likely due to the lipotoxicity induced by pure palmitate.[11] We therefore imaged and analyzed only cells that were still adherent. It can be seen that the number and size of lipid droplets is significantly lower compared to the two previous cases. It has previously been shown by Listenberfer *et al.*[11] that oleic acid is a necessary substrate to channel palmitic acid into cellular lipid droplets, and has been proposed as a mechanism of cells escaping palmitic acid induced lipotoxicity. However, until now it has not been shown that this event indeed happens on the single lipid droplet level, which clearly becomes apparent in our analysis. One can also compare the relative palmitic acid content in cells treated with pure oleic acid, which is ~10%, to the content of 18:1 fatty acids in cells that are treated with pure palmitic acid, which is ~26%. This result shows that 18:1 fatty acids are about twice as important as a substrate for lipid droplets as is palmitic acid. This notion is also true for the opposite case when looking at the 18:1 fatty acids content of cells that were treated with pure oleate, which is ~80%, in comparison with the palmitic acid content in cells that were treated with pure palmitate, which is ~49%. This, again, is supporting the notion that 18:1 fatty acids are the preferable substrate for intracellular lipid droplets. Fig. 3d shows the CARS image of untreated control cells. Here, only very few cellular lipid droplets are present, as compared to any of the treatment cases. The size of the droplets is also significantly smaller than in the treated cells. In control cells the relative amount of 18:1 fatty acids are also much higher compared to the relative amount of palmitic acid, indicating that this imbalance is present in a natural state of the cell.

We have shown that based on our approach it is possible to determine the composition of individual cellular lipid droplets in cells. There are, however, other cellular organelles that are involved in lipid-metabolism, that should also provide a detectable lipid signal. Peroxisomes, for example, are essential energy producing organelles, performing β-oxidation of excessive cellular fatty acids in cells.[34] For this reason we tried to determine if individual cellular peroxisomes can also produce a notable CARS signal and lipid Raman spectrum that can be distinguished from that of LDs.

We used our combined multiphoton microscope and Raman spectrometer to investigate cellular peroxisomes in untreated HepG2 cells in order to avoid the background of large numbers of lipid droplets induced by fatty acid treatment. Cells were imaged on the multiphoton microscope 24 h after the transfection with the GFP-peroxisome marker. The CARS signal from cellular lipid droplets, and the two-photon excitation fluorescence (TPEF) signal from GFP-labeled peroxisome were simultaneously detected on

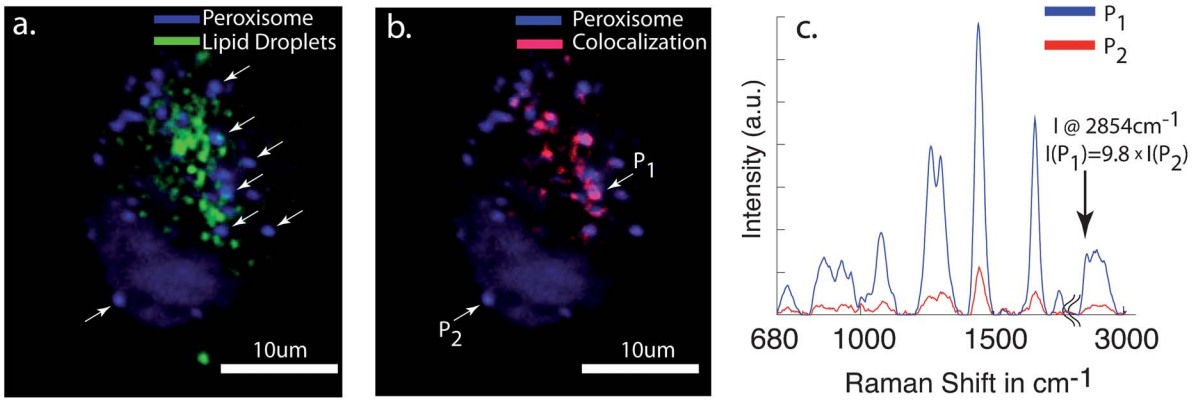

Fig. 4 (a) An overlay of CARS and TPEF images showing cellular lipid droplets (green) and peroxisomes (blue), respectively. The arrows indicate the locations of peroxisomes where Raman spectra were taken. (b) shows the colocalization analysis between the TPEF image of peroxisome, and the CARS image of lipid droplets. The red regions indicate areas of high colocalization. (c) shows the not-normalized spectra acquired at P_1 and P_2, visualizing the difference in intensity between areas of the TPEF and the CARS image that are colocalized. The arrow indicates the CH_2 stretch vibration 2854 cm^{-1} used for our CARS imaging, and the intensity difference between P_1 and P_2.

individual photomultiplier channels. Fig. 4a shows the combined CARS and TPEF image of cellular lipid deposits and the peroxisome distribution in a HepG2 cell. After the images were acquired, Raman spectra were taken from multiple peroxisomes within the cells, as indicated by the white arrows in Fig. 4a. Due to the near-IR wavelength of the continuous-wave laser used to excite Raman scattering no background fluorescence signal from the GFP-labeled peroxisomes was generated. Because of the low signal intensity the acquisition time for the spectra of peroxisome had to be increased to 30 s. Some overlap between the TPEF signal from peroxisome and the CARS signal from lipid droplets can be seen. To better visualize the colocalization between the two signals both images were multiplied, and overlaid with the TPEF image of peroxisomes, see Fig. 4b. Different degrees of colocalization between the CARS and the TPEF signal can be seen, supporting the assumption that some of the CARS signal is generated from peroxisomes. To investigate why not all peroxisomes show a CARS signal we compared the absolute Raman spectra of peroxisomes that show high colocalization between the CARS and the TPEF signal, with peroxisomes that show little colocalization between the CARS and the TPEF signal, see Fig. 4c (also highlighted by arrows in Fig. 4b). The intensity of the CH_2 stretch vibration at 2854 cm^{-1} is 9.8 times stronger for areas of high colocalization as compared to areas of low colocalization. Moreover, it has to be considered that the spontaneous Raman signal intensity is linearly dependent on the number of scatterers, whereas CARS is quadratically dependent on the number of scatterers. This leads to a signal difference between the highly colocalized CARS signal and the not localized CARS signal of a factor of 96, explaining why not every peroxisome shows up in the CARS image. We fitted the normalized Raman spectra of peroxisomes indicated in Fig. 4a with the spectrum of pure oleic acid, as we did with cellular lipid droplets. We find that 18:1 fatty acid (oleic and vaccenic acid) are present at (74% $\pm$ 4%) in the evaluated peroxisomes, which is twice as high as compared to the 18:1 fatty acid content in cellular lipid droplets in control cells. Based on the small standard error it is apparent that there is very little compositional difference between peroxisomes.

4 Conclusion

To our knowledge we have shown for the first time that by using CARS microscopy in conjunction with Raman micro-spectroscopy and asymmetric least squares fitting, we can determine the percentile amount of fatty acids of interest in single cellular lipid droplets. By comparing our results from single lipid droplet measurements to the results of the analysis of lipid droplets from millions of cells by gas chromatography we find that the fatty acid content when averaging spectra from several individual cellular lipid droplets is reflected in the bulk sample. Moreover, this method supports the previously proposed lipotoxicity protection pathway that oleic acid likely channels palmitic acid into the cellular lipid droplets, because we find that oleic acid and palmitic acid are always present in the same lipid droplets, and the relative ratio between the two fatty acids changes according to the amount with which the cells were treated. Furthermore, by imaging the distribution of cellular lipid droplets with CARS microscopy and imaging the distribution of peroxisomes we find that both organelles can reside in close proximity to each other, and, by taking Raman spectra from peroxisomes we find that they contain almost twice as much 18:1 fatty acids as lipid droplets in comparable cells. This approach opens a new way of investigating cellular lipid droplets and peroxisomes and can be extended to the analysis of more complex samples, treated with multiple fatty acid types under different physiological conditions.

Acknowledgements

We would like to acknowledge support by the National Institutes of Health, National Cancer Institute, under grant number 1U54CA136465-01. Lena Nolte was supported by a RISE fellowship from the German Academic Exchange Service (DAAD). This work was also supported in part by funding from the National Science Foundation. The Center for Biophotonics, an NSF Science and Technology Center, is managed by the University of California, Davis, under Cooperative Agreement no. PHY

0120999. We would like to thank William R. Keyes of the USDA-ARS-WHNRC for technical assistance with GC-MS analyses. This work was funded in part by the following: intramural USDA-ARS Project 5306-51530-000-19D (J.W.N). The USDA is an equal opportunity employer and provider.

References

1 T. Fujimoto, Y. Ohsaki, J. Cheng, M. Suzuki and Y. Shinohara, *Histochem. Cell Biol.*, 2008, **130**, 263–279.
2 R. V. Farese Jr and T. C. Walther, *Cell*, 2009, **139**, 855–860.
3 A. Pol, S. Martin, M. A. Fernandez, C. Ferguson, A. Carozzi, R. Luetterforst, C. Enrich and R. G. Parton, *Mol. Biol. Cell*, 2004, **15**, 99–110.
4 S. Martin and R. G. Parton, *Nat. Rev. Mol. Cell Biol.*, 2006, **7**, 373–378.
5 T. Fujimoto, H. Kogo, K. Ishiguro, K. Tauchi and R. Nomura, *J. Cell Biol.*, 2001, **152**, 1079.
6 M. A. Welte, *Trends Cell Biol.*, 2007, **17**, 363–369.
7 S. Sato, M. Fukasawa, Y. Yamakawa, T. Natsume, T. Suzuki, I. Shoji, H. Aizaki, T. Miyamura and M. Nishijima, *J. Biochem.*, 2006, **139**, 921.
8 G. Barba, F. Harper, T. Harada, M. Kohara, S. Goulinet, Y. Matsuura, G. Eder, Z. Schaff, M. J. Chapman and T. Miyamura, *Proc. Natl. Acad. Sci. U. S. A.*, 1997, **94**, 1200.
9 J. McLauchlan, M. K. Lemberg, G. Hope and B. Martoglio, *EMBO J.*, 2002, **21**, 3980–3988.
10 J. Goodman, *J. Biol. Chem.*, 2008, **283**, 28005.
11 L. L. Listenberger, X. Han, S. E. Lewis, S. Cases, R. V. Farese, D. S. Ory and J. E. Schaffer, *Proc. Natl. Acad. Sci. U. S. A.*, 2003, **100**, 3077–3082.
12 Y. Wei, D. Wang, F. Topczewski and M. Pagliassotti, *Am. J. Physiol.: Endocrinol. Metab.*, 2006, **291**, E275–E281.
13 D. Wang, Y. Wei and M. Pagliassotti, *Endocrinology*, 2006, **147**, 943.
14 C. L. Evans, E. O. Potma, M. Puoris'haag, D. Côté, C. P. Lin and X. S. Xie, *Proc. Natl. Acad. Sci. U. S. A.*, 2005, **102**, 16807–16812.
15 X. Nan, E. O. Potma and X. S. Xie, *Biophys. J.*, 2006, **91**, 728–735.
16 T. Hellerer, C. Axäng, C. Brackmann, P. Hillertz, M. Pilon and A. Enejder, *Proc. Natl. Acad. Sci. U. S. A.*, 2007, **104**, 14658.
17 T. Weeks, I. W. Schie, L. den Hagen, J. Rutledge and T. Huser, *J. Biomed. Opt.*, 2011, **16**, 0211171–0211175.
18 I. W. Schie, J. Wu, T. Weeks, M. A. Zern, J. C. Rutledge and T. Huser, *J. Biophotonics*, 2011, **4**, 425–434.
19 M. N. Slipchenko, T. T. Le, H. Chen and J. X. Cheng, *J. Phys. Chem. B*, 2009, **113**, 7681–7686.
20 H. A. Rinia, K. N. J. Burger, M. Bonn and M. Müller, *Biophys. J.*, 2008, **95**, 4908–4914.
21 J. Wu, K. Karlsson and Å. Danielsson, *J. Hepatol.*, 1997, **26**, 669–677.
22 E. A. Wiemer, T. Wenzel, T. J. Deerinck, M. H. Ellisman and S. Subramani, *J. Cell Biol.*, 1997, **136**, 71–80.
23 I. W. Schie, T. Weeks, G. P. McNerney, S. Fore, J. K. Sampson, S. Wachsmann-Hogiu, J. C. Rutledge and T. Huser, *Opt. Express*, 2008, **16**, 2168–2175.
24 T. Pologruto, B. L. Sabatini and K. Svoboda, *Biomed. Eng.*, 2003, **2**, 13.
25 C. Lieber and A. Mahadevan-Jansen, *Appl. Spectrosc.*, 2003, **57**, 1363–1367.
26 B. Beier and A. Berger, *Analyst*, 2009, **134**, 1198–1202.
27 F. Smedes, *Analyst*, 1999, **124**, 1711–1718.
28 K. Shafer-Peltier, A. Haka, M. Fitzmaurice, J. Crowe, J. Myles, R. Dasari and M. Feld, *J. Raman Spectrosc.*, 2002, **33**, 552–563.
29 N. Stone, M. Hart Prieto, P. Crow, J. Uff and A. Ritchie, *Anal. Bioanal. Chem.*, 2007, **387**, 1657–1668.
30 J. C. Hamilton and P. J. Gemperline, *J. Chemom.*, 2005, **4**, 1–13.
31 H. F. Boelens, R. J. Dijkstra, P. H. Eilers, F. Fitzpatrick and J. A. Westerhuis, *J. Chromatogr., A*, 2004, **1057**, 21–30.
32 J. W. Chan, D. Motton, J. C. Rutledge, N. L. Keim and T. Huser, *Anal. Chem.*, 2005, **77**, 5870–5876.
33 C. Chow, *Fatty acids in foods and their health implications*, CRC, 2008, vol. 170.
34 Y. Poirier, V. D. Antonenkov, T. Glumoff and J. K. Hiltunen, *Biochim. Biophys. Acta, Mol. Cell Res.*, 2006, **1763**, 1413–1426.

